

Cross-correlations between signal's components

Quankun Zhao(赵全坤), Sen Li(李森), Changgui Gu(顾长贵), Haiying Wang(王海英), and Huijie Yang(杨会杰)
Citation: Chin. Phys. B, 2025, 34 (**2**): 028702. DOI: 10.1088/1674-1056/ad9ffb
Journal homepage: http://cpb.iphy.ac.cn; http://iopscience.iop.org/cpb

What follows is a list of articles you may be interested in

A new viewpoint and model of neural signal generation and transmission: Signal transmission on myelinated neuron

Zuoxian Xiang(向左鲜), Chuanxiang Tang(唐传祥), Lixin Yan(颜立新), Chao Chang(常超)†, and Guozhi Liu(刘国治)‡
Chin. Phys. B, 2020, 29 (**10**): 108701. DOI: 10.1088/1674-1056/abaee9

Wavelet optimization for applying continuous wavelet transform to maternal electrocardiogram component enhancing

Qiong Yu(于琼), Qun Guan(管群), Ping Li(李萍), Tie-Bing Liu(刘铁兵), Jun-Feng Si(司峻峰), Ying Zhao(肇莹), Hong-Xing Liu(刘红星), Yuan-Qing Wang(王元庆)
Chin. Phys. B, 2017, 26 (**11**): 118702. DOI: 10.1088/1674-1056/26/11/118702

Some regularity on how to locate electrodes for higher fECG SNRs

Zhang Jie-Min (张洁敏), Huang Xiao-Lin (黄晓林), Guan Qun (管群), Liu Tie-Bing (刘铁兵), Li Ping (李萍), Zhao Ying (肇莹), Liu Hong-Xing (刘红星)
Chin. Phys. B, 2015, 24 (**3**): 038702. DOI: 10.1088/1674-1056/24/3/038702

Trends in ultrashort and ultrahigh power laser pulses based on optical parametric chirped pulse amplification

Xu Lu (徐露), Yu Liang-Hong (於亮红), Chu Yu-Xi (储玉喜), Gan Ze-Biao (甘泽彪), Liang Xiao-Yan (梁晓燕), Li Ru-Xin (李儒新), Xu Zhi-Zhan (徐至展)
Chin. Phys. B, 2015, 24 (**1**): 018704. DOI: 10.1088/1674-1056/24/1/018704

Cardiac electrical activity imaging of patients with CRBBB or CLBBB in magnetocardiography

Zhu Jun-Jie (朱俊杰), Jiang Shi-Qin (蒋式勤), Wang Wei-Yuan (王伟远), Zhao Chen (赵晨), Wu Yan-Hua (吴燕华), Luo Ming (罗明), Quan Wei-Wei (权薇薇)
Chin. Phys. B, 2014, 23 (**4**): 048702. DOI: 10.1088/1674-1056/23/4/048702

Cross-correlations between signal's components

Quankun Zhao(赵全坤), Sen Li(李森), Changgui Gu(顾长贵),
Haiying Wang(王海英), and Huijie Yang(杨会杰)†

Department of Systems Science, University of Shanghai for Science and Technology, Shanghai 200093, *China*

(Received 21 October 2024; revised manuscript received 30 November 2024; accepted manuscript online 17 December 2024)

Detecting coupling pattern between elements in a complex system is a basic task in data-driven analysis. The trajectory for each specific element is a cooperative result of its intrinsic dynamic, its couplings with other elements, and the environment. It is subsequently composed of many components, only some of which take part in the couplings. In this paper we present a framework to detect the component correlation pattern. Firstly, the interested trajectories are decomposed into components by using decomposing methods such as the Fourier expansion and the Wavelet transformation. Secondly, the cross-correlations between the components are calculated, resulting into a component cross-correlation matrix (network). Finally, the dominant structure in the network is identified to characterize the coupling pattern in the system. Several deterministic dynamical models turn out to be characterized with rich structures such as the clustering of the components. The pattern of correlation between respiratory (RESP) and ECG signals is composed of five sub-clusters that are mainly formed by the components in ECG signal. Interestingly, only 7 components from RESP (scattered in four sub-clusters) take part in the realization of coupling between the two signals.

Keywords: coupling structure, cross-correlation matrix, component correlation network

PACS: 87.85.Ng, 64.60.aq, 11.15.Me

DOI: 10.1088/1674-1056/ad9ffb **CSTR:** 32038.14.CPB.ad9ffb

1. Introduction

A complex system is composed of several or many elements. Each element is an agent that has its own specific dynamical behavior. The agents interact with each other by complicated couplings between them, resulting into a network. This network accompanying with the environments determines the system's dynamical process, records for which form a multivariate time series.[1] The inter-dependence between the records, called correlation, in return can shed light on the underlying dynamical mechanism and be helpful for evaluation, prediction, intervention, and even controlling of the system.[2] Correlation in spatial-temporal records attracts accordingly persistent attentions from diverse research fields.[3–7]

The correlation in temporal dimension presents us memory behavior. Within each specific time series, the inter-dependence between records separated by a specific time delay is currently measured by means of, e.g., the Pearson correlation coefficient and the conditional entropy.[8–10] When the relation of dependence versus time delay decays exponentially, the memory has a characteristic length, termed short-range correlation.[11] In a large amount of complex systems in diverse fields from physiology, society, finance, to ecology, the relation decays according to a power-law instead of the exponential one, termed long-range correlation.[12,13]

The correlation in spatial dimension gives us the coupling effects between observable quantities. All the cross-correlations between the observable quantities measured with, e.g., the Pearson correlation coefficient and the mutual entropy, form a correlation-matrix (graph). Properties of the graph defined in network theory and random matrix theory[14,15] give us profound insights on the state and evolution of the complex system. For instances, the eigenvectors corresponding to the largest and the second eigenvalues of the matrix can cluster stocks into reasonable groups.[16,17] Though the density of its spectrum obeys a semi-circle law, there usually appears a peak of density centered at a large eigenvalue.[18] The components in the eigenvector corresponding to the center of the peak provide us information for the system's collective motion. And the average linkage density in the graph for ten stock markets predicts successfully financial crises.[19]

Generally speaking, there exist nontrivial patterns in the temporal-spatial records at different scales, and the patterns are dependent with each other in the temporal and spatial dimensions. The dependence between the patterns provides us the hyper details of correlation, called correlation structure herein.[20] However, the currently used concepts such as the (cross-)correlation coefficient and the mutual entropy share a procedure of statistical average, where details of correlation structure are merged into scalar quantities, i.e., the structure information is lost. To preserve the microscopic details of correlation people have proposed various solutions to map temporal-spatial records into networks, paving a new way to characterize dynamical systems.[21] For a multivariate time

†Corresponding author. E-mail: hjyang@ustc.edu.cn

© 2025 Chinese Physical Society and IOP Publishing Ltd. All rights, including for text and data mining, AI training, and similar technologies, are reserved.

series, a straight-forward strategy is to construct the correlation matrix and interpret it as the adjacency matrix for a network.[22–24] For a mono-variate time series, one can map the series segments each to nodes, and adopt the distances between them as linking weights between the nodes.[25–27] Alternatively, the records each are mapped to nodes, and a pair of nodes are linked only when they can see each other, i.e., all the records between them are under the straight line linking them.[28–30] The networks corresponding to all the observable quantities form a multi-layer network. This network based temporal-spatial series analysis has made fruitful achievements. For instances, the network constructed from meteorological data[31] reveals that the coupling strengths between different regions diverse in a wide range, resulting into some clusters with tightly intra-linkages and loosely inter-linkages. The network mapped from temperature data[32] exposes the important role of ocean surface circulation in stabilising the global long-term temperature field. And the global coupling pattern of extreme rainfall events is identified successfully in the network constructed from high-resolution satellite data.[33]

In this work we investigate the correlation structure stored in components of signals, called component correlation network. It is stimulated by two facts. First, the records for a specific observable quantity form a mono-variate time series, but it is actually a cooperative result of dynamical processes for all the agents in the system. For instance, one can monitor a person's healthy state with a multi-channel signal composing of the heat-beat series, the EEG signals in brain, the respiration series, and the eye-ball motions, etc.[34–37] The heartbeat series, e.g., is widely used to represent the healthy state of the heart, but it is generated by different organs networked by their inter-influences. It contains accordingly contributions from all the organs. Second, the agents each have their own intrinsic behaviors. Let us take also the human body as an example. The body's biological rhythm is about 24 hours. The heart-beat and respiration have a characteristic period of about 1 second. While the EEG signals emitted from brain have a characteristic period of about 10^{-3} or even 10^{-4} second. The network of organs works in a wide range of characteristic periods covering a total of 8 orders of magnitude. A general mechanism for realization of coupling between two agents with different characteristic periods is the resonance between their components with close periods.[38,39] The components in a time series may tell us the contributions from different agents, and how the influence between each pair of the agents occurs.

To find the component correlation structure, we decompose the time series for interested observable quantities into components, taken as the contributions from all the agents. And then we calculate the cross-correlations between all the pairs of components, which form the component correlation matrix. The correlations between the components for a specific time series give us the intra-correlation behavior for the corresponding observable quantity. And the correlations between the components come from different time series provide us the inter-correlation behavior for the corresponding observable quantities.

Technically, the Fourier expansion and the wavelet decomposition are used to obtain the components. For the components obtained with the Fourier expansion, each component has a specific oscillation angle speed and an expansion coefficient, denoted with a vector in polar coordinate system. The correlation between a pair of components is quantified with the absolute value of the scalar product of their corresponding vectors. For the components obtained with the wavelet decomposition, each component is a series of expansion coefficients, forming a high-dimensional vector. The correlation between a pair of components is quantified with the absolute value of the scalar product of the corresponding two high-dimensional vectors.

As an illustration, we investigated time series generated with several typical chaotic dynamic models and two physiological signals. The number of retained frequency components has a strong and positive correlation with the Lyapunov exponent. The components tend to group into clusters, providing us with rich patterns of correlations between variables in the systems each. In the empirical example of the ECG and RESP signals, the frequency components in ECG signal group into five sub-clusters, four in which are coupled with a total of 7 frequency components in RESP, respectively.

2. Method

The discrete Fourier transform is used to find the components with different oscillation frequencies. Let us consider a time series with a length of N, $F \equiv \{f_0, f_2, \ldots, f_{N-1}\}$. Assuming F is absolutely summable, i.e., the summation for the absolutes of its elements is finite $\sum_{n=0}^{N-1} |f_n| < \infty$, its expansion reads,

$$f_n = \frac{1}{N}\sum_{k=0}^{N-1} X(k)\exp\left(\mathrm{i}\frac{2\pi}{N}kn\right), \quad n = 1,2,\ldots,N-1, \quad (1)$$

where X_k, $k = 0,1,2,\ldots,N-1$, the expansion coefficients corresponding to the waves of

$$\left\{\exp\left(\mathrm{i}\frac{2\pi}{N}kn\right), \quad k = 0,1,2,\ldots,N-1; \quad n = 0,1,2,\ldots,N-1\right\}$$

read

$$X(k) = \sum_{n=1}^{N-1} f_n \exp\left(-\mathrm{i}\frac{2\pi}{N}kn\right), \quad k = 0,2,\ldots,N-1, \quad (2)$$

called frequency components for the series F. Re-arranging the power spectral densities of the components

$$\frac{|X(k)|^2}{\sum_{m=1}^{N-1}|X(m)|^2}, \quad k = 1,2,\ldots,N-1$$

in a descending order, the frequency components whose accumulative power spectral density reaches a specified value (in this work it is chosen to be 0.9) are preserved as the considered components, and the other components are discarded. The retained components with frequencies from high to low are assigned the identification numbers of $1,2,\ldots,k$.

Each frequency component, e.g., the k-th one can be represented with two pieces of information,[40]

$$\begin{aligned} A(k) &= |X(k)|, \\ \phi(k) &= \arg(X(k)), \end{aligned} \tag{3}$$

describing its amplitude (contribution to F) and its oscillation speed, respectively. The frequency component correlation matrix R^{f} is accordingly defined as

$$R^{\mathrm{f}}_{mn} = |A(m)A(n)|\cos[\phi(m)-\phi(n)], \quad m,n = 1,2,\ldots,M, \tag{4}$$

i.e., each entity is the scalar product between the corresponding vectors, where M is the total number of the retained components. In calculations the algorithm of Fast Fourier transform[41,42] is adopted.

The components corresponding to different scales, called scaling components, are found also by means of the continuous wavelet transform. Expanding the time series F with a set of wavelets $\psi\left(\frac{n-b}{a}\right)$, $n = 0,1,2,\ldots,N-1$,

$$f_n \sim \sum_{a=a_1}^{a_M}\sum_{b=0}^{N-1} W(a,b)\psi\left(\frac{n-b}{a}\right), \quad n = 1,2,\ldots,N-1, \tag{5}$$

where a is the scale selected to be $a_1,a_2,\ldots,a_M$, and $b = 0,2,\ldots,N-1$ the translation of the center for the wavelet. And $W(a,b)$ is the expansion coefficient (contribution to F) obtained with

$$W(a,b) = \frac{1}{\sqrt{a}}\sum_{n=0}^{N-1} F(k)\psi\left(\frac{n-b}{a}\right). \tag{6}$$

For each specific scale a, all the expansion coefficients $W(a,b), b = 0,1,2,\ldots,N-1$ form a vector, representing the component corresponding to the scale a. In order to capture more detailed frequency information, we decompose each signal on 32 scales, and the obtained scaling components are thus numbered from scale 1 to scale 32. In calculations the Mexican hat wavelet is adopted.[43,44]

For a pair of scaling components with scales, e.g., a_m and a_n, one calculates the time-delayed correlations

$$C_{mn}(\tau) = \sum_{b=0}^{N-\tau} W(a_m,b)W^*(a_n,b,b+\tau), \tag{7}$$

where τ is a time delay in the range of $-(N-1) \le \tau \le +(N-1)$. The maximum one in the correlation values corresponding to different τ is regarded as the correlation strength between the component pairs, which generally not occurs at $\tau = 0$. The scale component correlation matrix R^{w} reads

$$\begin{aligned} R^{\mathrm{w}}_{mn} &= \max\{C_{a_m,a_n}(m), \\ &\tau = -(N-1), 2-N,\ldots,N-2,+(N-1)\}, \\ &m,n = 1,2,\ldots,M. \end{aligned} \tag{8}$$

Generally speaking, the the retained components group into different clusters, within (among) which there exist significantly large (small) average of correlation strength. From an obtained frequency/scaling component correlation matrix (R^{f} or R^{w}), one replaces all the entities with their absolutes, resulting into a component correlation strength matrix ($|R^{\mathrm{f}}|$ or $|R^{\mathrm{w}}|$). A heat-map is currently adopted to display its structure. To expose the clustering behavior we first construct a clustering-tree for the components by using the clustering tree algorithm, and then re-arrange the components to position those belonging to the same (sub-)clusters together, denoted with $s_1,s_2,\ldots,s_l$, respectively. The component correlation strength matrices are mapped also to networks, where the nodes and weights of edges are the components and the correlation strengths, respectively. To expose the dominant topological structure for each constructed network, a threshold t is introduced to filter out weak correlations.[45–48]

What is more, a specific variable's retained components that take part in the variable's couplings with other variables usually center around a specific frequency, called aggregation behavior. Without loss of generality, let us consider the retained components from the variable x in the (sub-)cluster named sub, denoted with $\{I_1,I_2,\ldots,I_v\}$, where v is the total number of the components. We randomly take out a sub-set containing a total of n identification numbers from the set of identification numbers for the retained components of the variable x, conducting which W times leads to a total of W subsets,

$$\begin{aligned} &I^{\mathrm{R}}_w = \left\{I^{\mathrm{R}}_w(1),I^{\mathrm{R}}_w(2),\ldots,I^{\mathrm{R}}_w(v)\right\} \subset \{1,2,\ldots,N_{\mathrm{sub}}\}, \\ &w = 1,2,\ldots,W. \end{aligned}$$

The aggregation behavior for the retained components from x in the (sub-)cluster sub is measured with

$$G^{\mathrm{sub}}_x \equiv \frac{\sum_{i\neq j=1}^{v}|I_i - I_j|}{\frac{1}{W}\sum_{w=1}^{W}\sum_{i\neq j=1}^{v}|I^{\mathrm{R}}_w(i) - I^{\mathrm{R}}_w(j)|}, \tag{9}$$

called aggregation degree. In calculations W is chosen to be 1000. A smaller value of G^{sub}_x implies the frequencies for the retained components distributed around a specific frequency in a sharper interval.

The structural behavior for each specific component, e.g., the n-th frequency component, is measured with its entropy E^{f}_n and participation ratio Q^{f}_n, defined as

$$E^{\mathrm{f}}_n \equiv -\frac{1}{\ln M}\sum_{k=1}^{M}\frac{|R^{\mathrm{f}}_{kn}|}{\sum_{s=1}^{M}|R^{\mathrm{f}}_{sn}|}\ln\left\{\frac{|R^{\mathrm{f}}_{kn}|}{\sum_{s=1}^{M}|R^{\mathrm{f}}_{sn}|}\right\},$$

$$Q_n^{\mathrm{f}} \equiv \left\{ M \sum_{k=1}^{M} \left[\frac{|R_{kn}^{\mathrm{f}}|}{\sum_{s=1}^{M} |R_{sn}^{\mathrm{f}}|} \right]^2 \right\}^{-1}. \tag{10}$$

The value of E_n^{f} estimates the strength of correlations of the n-th frequency component with the others, while that for Q^{f} shows further the homogenous behavior of the correlations. The entropy and participation ratio for the n-th scaling components, denoted with E_n^{w} and Q_n^{w}, can be calculated with an analogous procedure. In the definition of entropy, a multiplier $1/\ln M$ is introduced to the Shannon entropy to be sure its value is in the range of $[0,1]$.

The computational procedure is illustrated in Fig. 1.

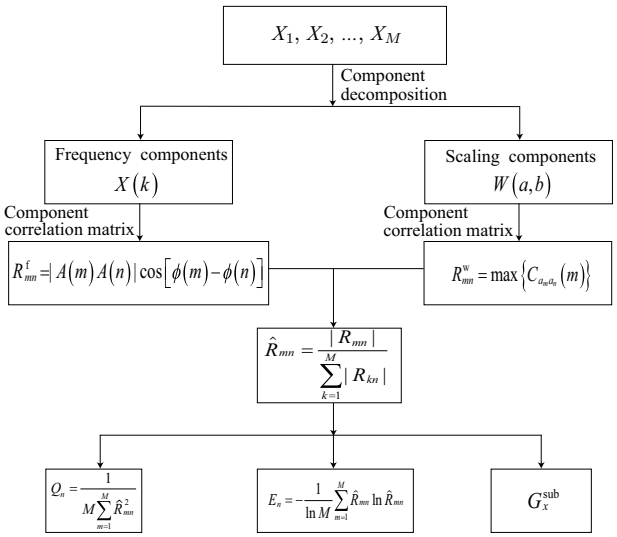


Fig. 1. The procedure for component correlaion analysis. First, one decomposes the considered mono/multi-variate time series into components by means of Fourier expansion or wavelet transformation. Second, the frequency and scaling component correlation matrices (networks) are constructed, from which one obtains their structural properties such as the clustering behavior. Last, every column is rescaled with the summation of all the entities in it, resulting into two new matrices (networks) in which the summation of the entities in every column is unitary, implying that the entities can be accordingly interpreted as probabilities. The nonhomogenous behaviors are subsequently measured with entropy and participation ratio.

3. Results

As typical examples, we investigate the chaotic trajectories generated by Henon map, logistic map, Lorentz system, and Rossler system.

3.1. Henon map

The Henon map reads

$$\begin{cases} x_{n+1} = 1 - \alpha x_n^2 + y_n, \\ y_{n+1} = \eta x_n. \end{cases} \tag{11}$$

The parameter η is selected to be 0.3, and the parameter α starts at 0.8 and ends at 1.4.

As shown in Fig. 2(a), the number of retained frequency components in x and y increases (decreases) significantly as the system evolves from a non-chaotic (chaotic) state to a chaotic (non-chaotic) one. Actually, a larger Lyapunov exponent implies also a larger number of frequency components.

For the chaotic trajectory generated with $(\alpha,\eta) = (1.3, 0.3)$ (the Lyapunov exponent is 0.11), the total of 346 retained frequency components in x and y cluster into 6 sub-clusters denoted with s_1, s_2, s_3, s_4, s_5, and s_6 (see the heat-map in Fig. 2(b)). There exist limited linkages between the sub-clusters s_2 and s_3, however they both each are strongly connected with s_1 respectively, resulting into a cluster centered at s_1, named with S_A. There exist limited linkages between the sub-clusters s_4 and s_6, however they both each are strongly connected with s_5 respectively, resulting into a cluster centered at s_5, named with S_B. The clusters S_A and S_B are linked by the sub-cluster s_2. Table 1(a) presents the numbers of retained frequency components in the (sub-)clusters each and their aggregation behaviors. The frequencies for the components from y in sub-cluster s_5 aggregate more tightly compared with that in the other sub-clusters.

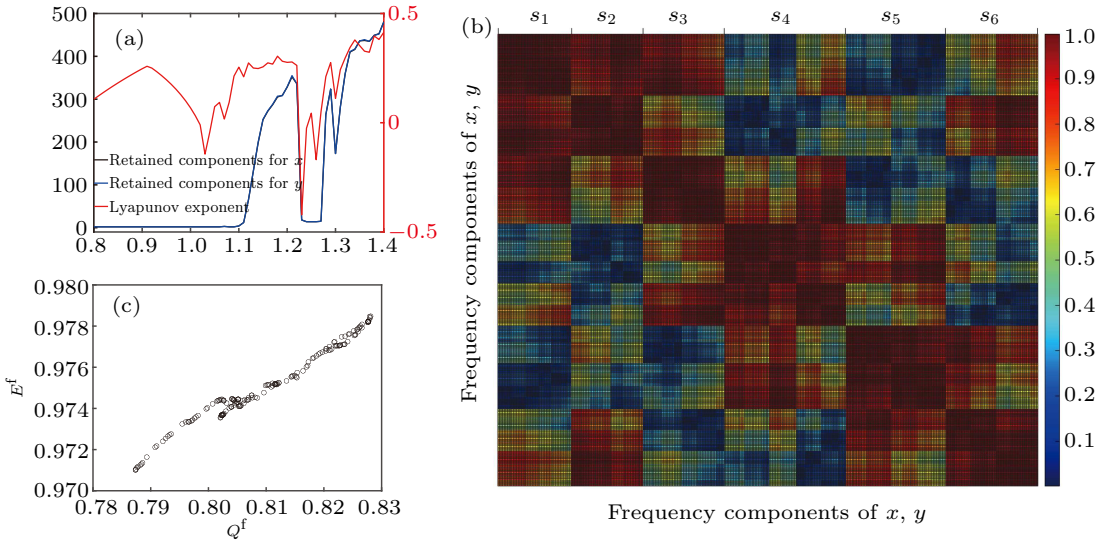


Fig. 2. Correlation between frequency components of the Henon map. (a) The curves of the retained frequency components of the x, y and the Lyapunov exponential curve with parameters α, respectively. (b) The clustering heat-map of components in the correlation strength matrix $|R^{\mathrm{f}}|$. The components from x, y are numbered in order from 1 to 346. (c) The scatter plot of entropy and participation ratio for each component.

Table 1. Percentage of components and aggregation degree in each sub-cluster for Henon map.

(a) Frequency components				
Sub	Components from x	G_x^{sub}	Components from y	G_y^{sub}
s_1	29/47	0.9005	18/47	0.9514
s_2	22/46	1.0267	24/46	0.9947
s_3	21/52	1.0114	31/52	1.0436
s_4	39/78	1.0553	39/78	0.9678
s_5	38/64	0.9597	26/64	0.8971
s_6	24/59	1.0232	35/59	0.9921
(b) Scaling components				
Sub	Components from x	G_x^{sub}	Components from y	G_y^{sub}
s_1	6/12	0.2117	6/12	0.2146
s_2	15/30	0.5233	15/30	0.5192
s_3	4/8	0.4844	4/8	0.4856
s_4	7/14	0.3247	7/14	0.3210

Figure 2(c) gives the entropy and participation ratio for each component. The maximum values of Q^{f} and E^{f} are 0.8281 and 0.9785, whose corresponding components are the the ones numbered 145 and 144 from x, respectively. These two frequency components are the hubs of the network, i.e., they have the largest number of neighbors.

For the chaotic trajectory generated with $(\alpha,\eta) = (1.3,0.3)$, the absolute values of the wavelet coefficients for the scaling components in x (upper part) and y (lower part) are presented in Fig. 3(a), respectively. The scaling components group into four sub-clusters marked with s_1, s_2, s_3, and s_4, where s_2 is a center that have strong linkages with s_1, s_3, and s_4, respectively (see the heat-map for $|R^{\text{w}}|$ in panel (b)). And the sub-clusters s_1, s_3, and s_4 are almost isolated with each other. Table 1(b) gives the numbers of scaling components in the sub-clusters each and their aggregation behaviors, from which one can find that the scaling components with successive scales aggregate tightly together in the sub-clusters each. Most of the points for $(Q^{\text{w}}, E^{\text{w}})$ aggregate at the up-right corner, i.e., their values are large (panel (c)). The maximum values of Q^{w} and E^{w} are 0.8712, 0.9874, whose corresponding components are the the ones numbered 14 from x and numbered 46 from y, respectively. The scaling components numbered 14, 46 take as the hubs of the network.

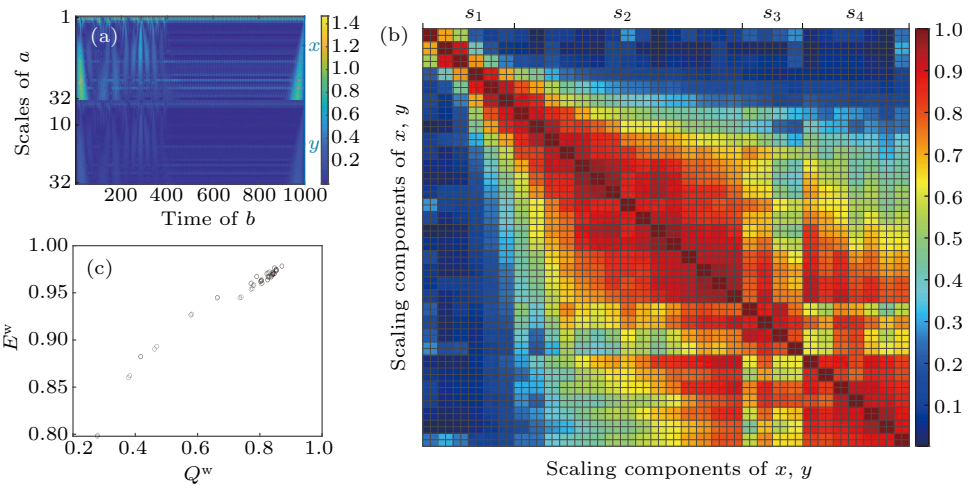


Fig. 3. Correlation between scaling components of the Henon map. (a) The absolute values of the wavelet coefficients for x and y on 32 scales, respectively. The components from x, y are numbered in order from 1 to 64. (b) The clustering heat-map of components in the correlation strength matrix $|R^{\text{w}}|$. (c) The scatter plot of entropy and participation ratio for each component.

3.2. Logistic map

The logistic map reads

$$x_{n+1} = rx_n(1-x_n). \tag{12}$$

The parameter r starts at 2.5 and ends at 4.

The number of retained frequency components in x at different values of parameter r are shown in Fig. 4(a1). When $r >$ 3.74, the number of retained frequency components increases (decreases) with the system evolves from a non-chaotic (chaotic) state to a chaotic (non-chaotic) state. A stronger (weaker) chaotic behavior measured with a larger/smaller Lyapunov exponent implies a larger (smaller) number of retained frequency components.

For the chaotic trajectory generated with $r = 3.8$ (the Lyapunov exponent is 0.44), the total of 25 retained frequency components in x cluster into 3 sub-clusters denoted with s_1, s_2, and s_3 (see the heat-map in Fig. 4(b1)). The frequency components in s_1 at the up-left corner are densely connected. The sub-cluster s_2 at the centre and the sub-cluster s_3 in the down-right corner composed of more small sub-clusters, respectively. As shown in Table 2, the aggregation degrees for the sub-clusters each are very close to 1, i.e., the frequency components from x in each sub-cluster are dispersed. Panel (c1) shows the entropy and participation ratio for all frequency components, in which most of the points for $(Q^{\text{f}}, E^{\text{f}})$ aggregate at the down-left corner, i.e., their values are small. The maximum values of Q^{f} and E^{f} are 0.8863, 0.9777, whose corresponding components both are the one numbered 1 from x. The frequency component numbered 1 takes as the hub of the network.

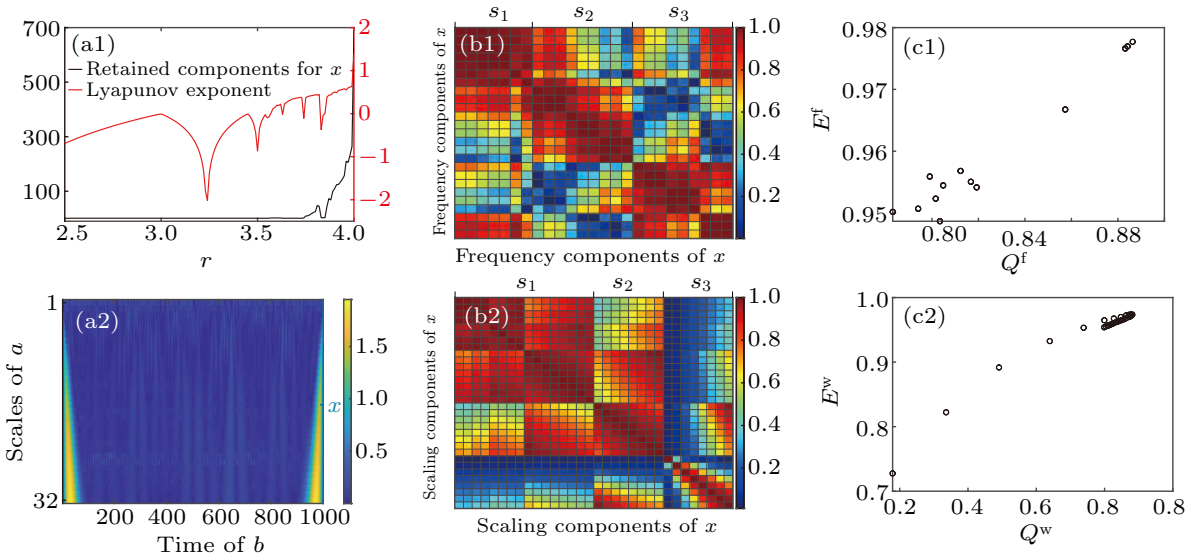


Fig. 4. Correlation between frequency [(a1)–(c1)]/scaling [(a2)–(c2)] components of the logistic map. (a1) The curves of the retained frequency components of the x and the Lyapunov exponential curve with parameters r, respectively. (b1) The clustering heat-map of components in the correlation strength matrix $|R^{\mathrm{f}}|$. The components from x are numbered in order from 1 to 25. (c1) The scatter plot of entropy and participation ratio for each component. (a2) The absolute values of the wavelet coefficients for x on 32 scales. The components from x are numbered in order from 1 to 32. (b2) The clustering heat-map of components in the correlation strength matrix $|R^{\mathrm{w}}|$. (c2) The scatter plot of entropy and participation ratio for each component.

Table 2. Percentage of components and aggregation degree in each sub-cluster for logistic map.

	Frequency components		Scaling components	
Sub	Components from x	G_x^{sub}	Components from x	G_x^{sub}
s_1	7	1.0584	16	0.5148
s_2	9	1.0217	8	0.2717
s_3	9	0.9784	8	0.2738

Figure 4(a2) provides the absolute values of the wavelet coefficients for the scaling components from x at different scales. In the clustering heat-map of the correlation strength matrix $|R^{\mathrm{w}}|$ in Fig. 4(b2), the scaling components cluster into 3 consecutive loose sub-clusters. The sub-clusters s_1 and s_2 are linked into a cluster, where the interacting components all originate from the components of x at different scales. Table 2 gives the numbers of scaling components in the sub-clusters each and their aggregation behaviors, showing that the scaling components with successive scales group tightly together in the sub-clusters each. As shown in panel (c2), the points of $(Q^{\mathrm{w}}, E^{\mathrm{w}})$ cluster at the up-right corner, where the values for them are large. The maximum values of Q^{w} and E^{w} are 0.8811, 0.9737, whose corresponding components are the ones numbered 14, 11 from x, respectively. These two scaling components numbered 14, 11 are the hubs of the network.

3.3. Lorentz system

The lorentz system reads

$$\begin{cases} \dot{x} = \sigma(y - x), \\ \dot{y} = x(\rho - z) - y, \\ \dot{z} = xy - \beta z. \end{cases} \tag{13}$$

The parameters σ and β are selected to be 10 and $8/3$, respectively, and the parameter ρ starts at 23 and ends at 200.

The number of retained frequency components in x, y, and z at different values of parameter ρ are shown in Fig. 5(a). The number of retained components in x and y exhibit similar trends as the Lyapunov exponent (red curve), i.e., it increases (decreases) significantly as the system evolves from a non-chaotic (chaotic) state to a chaotic (non-chaotic) one. But the number of retained frequency components in z exhibits a constant pattern.

For the chaotic trajectory generated with $(\sigma, \beta, \rho) = (10, 8/3, 199)$ (the Lyapunov exponent is 1.51), the total of 146 retained frequency components in x, y, and z cluster into 4 sub-clusters denoted with s_1, s_2, s_3, and s_4 (see the heat-map in Fig. 5(b)). The sub-clusters s_1 and s_3 both each are strongly connected with s_2, and all of them resualting into a cluster, which linked with sub-cluster s_4 by s_3. As shown in Table 3(a), the components from z do not appear in the sub-clusters s_1, s_2, s_3. And only one component from z appears in the sub-cluster s_4 (whose size is 59). The components from y have an aggregation degree close to 1 in each sub-cluster, while the frequencies for components from x in sub-cluster s_4 has the lowest aggregation, i.e., aggregating more tightly compared to those in the other sub-clusters. As shown in panel (c), the components with lower participation and entropy values are not significantly different in number from those with higher values. The maximum values of Q^{f} and E^{f} are 0.8337, 0.9755, whose corresponding components are the ones numbered 53, 54 from x, respectively. These two frequency components are the hubs of the network, i.e., they have the largest number of neighbors.

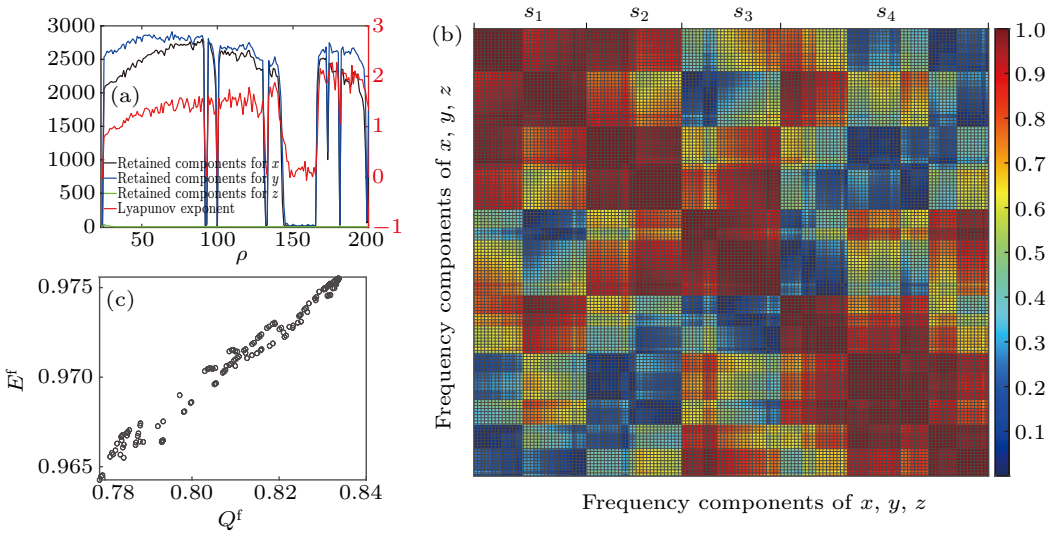


Fig. 5. Correlation between frequency components of the Lorentz system. (a) The curves of the retained frequency components of the x, y, and z, and the Lyapunov exponential curve with parameters ρ, respectively. (b) The clustering heat-map of components in the correlation strength matrix $|R^{\mathrm{f}}|$. The components from x, y, and z are numbered in order from 1 to 146. (c) The scatter plot of entropy and participation ratio for each component.

Table 3. Percentage of components and aggregation degree in each sub-cluster for Lorentz system.

(a) Frequency components

Sub	Components from x	G_x^{sub}	Components from y	G_y^{sub}	Components from z	G_z^{sub}
s_1	11/32	0.7769	21/32	0.9530	0	0
s_2	10/27	1.1479	17/27	1.1159	0	0
s_3	9/28	1.1264	19/28	0.8706	0	0
s_4	27/59	0.5866	31/59	0.9734	1/59	1

(b) Scaling components

Sub	Components from x	G_x^{sub}	Components from y	G_y^{sub}	Components from z	G_z^{sub}
s_1	26/52	0.8182	26/52	0.8194	0	0
s_2	6/12	0.2125	6/12	0.2116	0	0
s_3	0	0	0	0	32/32	1

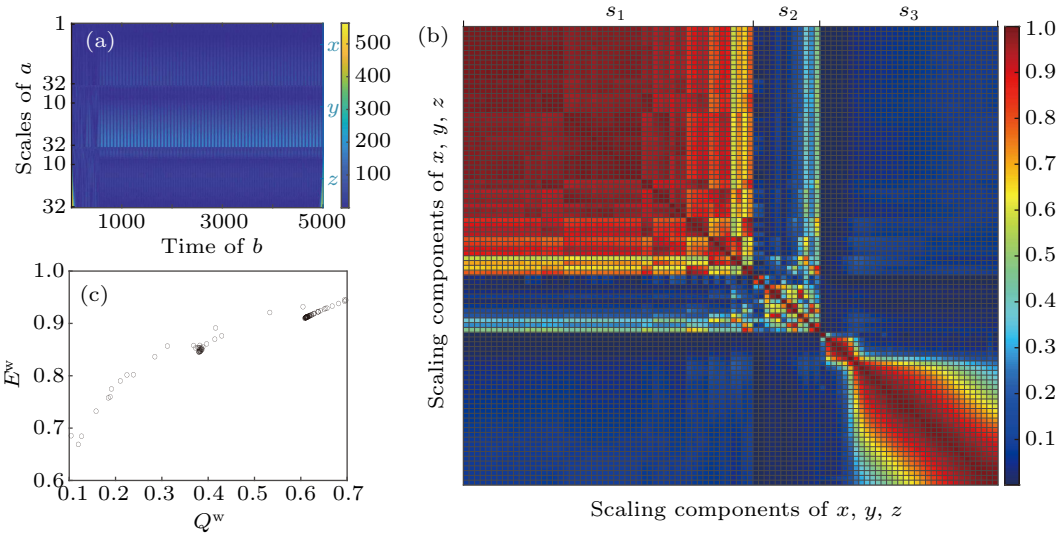


Fig. 6. Correlation between scaling components of the Lorentz system. (a) The absolute values of the wavelet coefficients for x, y, and z on 32 scales, respectively. (b) The clustering heat-map of components in the correlation strength matrix $|R^{\mathrm{w}}|$. The components from x, y, and z are numbered in order from 1 to 96. (c) The scatter plot of entropy and participation ratio for each component.

For the chaotic trajectory generated with $(\sigma,\beta,\rho) = (10, 8/3, 199)$, the absolute values of the wavelet coefficients for the scaling components in x (upper part), y (middle part), and z (lower part) are presented in Fig. 6(a), respectively. The scaling components group into 3 sub-clusters marked with s_1, s_2, and s_3, where the sub-cluster s_3 is almost completely isolated with sub-clusters s_1 and s_2 (see the heat-map for $|R^{\mathrm{w}}|$ in panel (b)). From Table 3(b), one can find that the com-

ponents in the sub-clusters s_1 and s_2 are mainly from x and y, while the components in s_3 are all from z with successive scales. The wavelet decomposition only can find the structure of cross-correlation between x and y, but failing between (x,z) or (y,z). As shown in Fig. 6(c), the points of $(Q^{\mathrm{w}},E^{\mathrm{w}})$ cluster mainly at the centre and upper-right corner, whereas components with smaller participation ratio and entropy value ,which have fewer neighbours in the network, occupy a minority. The maximum values of Q^{w} and E^{w} are 0.6974, 0.9449, whose corresponding components are the ones numbered 38 from y and numbered 6 from x, respectively. The scaling components numbered 38, 6 take as the hubs of the network.

3.4. Rossler system

The Rossler system reads

$$\begin{cases} \dot{x} = -(y+z), \\ \dot{y} = x+\mu y, \\ \dot{z} = \nu + z(x-\xi). \end{cases} \tag{14}$$

The parameters μ and ν are selected to be 0.2 and 0.2, respectively, and the parameter ξ starts at 4 and ends at 7.

As shown in Fig. 7(a), the black and blue curves representing the number of retained frequency components in x and y, respectively, show extremely similar trends, but a different trend from that of retained frequency components in z. And the number of retained components in x and y at each parameter ξ is much smaller than z.

For the chaotic trajectory generated with $(\mu,\nu,\xi) = (0.2,0.2,6.8)$ (the Lyapunov exponent is 1.51), the total of 201 retained frequency components in x, y, and z cluster into 4 sub-clusters denoted with s_1, s_2, s_3, and s_4 (see the heat-map in Fig. 7(b)). The components in sub-clusters s_3 act as a centre to connect sub-clusters s_2 and s_4, where there are limited weak connections, and similar behaviour occurs in s_2, which connecting sub-clusters s_1 and s_3. Table 4(a) presents the numbers of retained frequency components and their aggregation behaviors in the (sub-)clusters each. In each sub-cluster, most of the frequency components are from z. The frequencies for the components from x in sub-cluster s_3 aggregate more tightly compared to those in the other sub-clusters. Figure 7(c) gives the entropy and participation ratio for each component. The maximum values of Q^{f} and E^{f} are 0.8212, 0.9747, whose corresponding components are both the ones numbered 89 from z. The frequency component numbered 89 takes as the hub of the network.

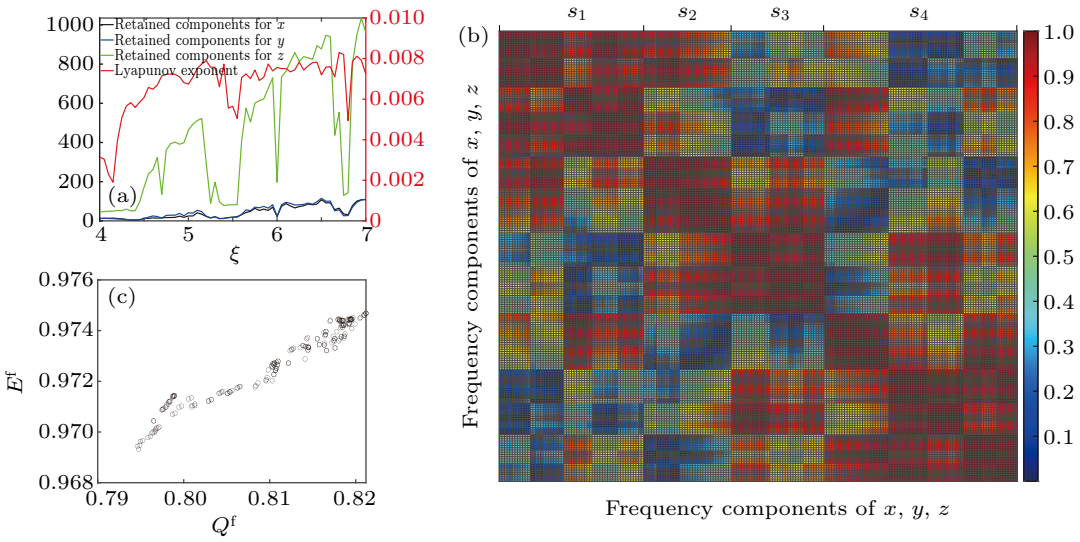


Fig. 7. Correlation between frequency components of the Rossler system. (a) The curves of the retained frequency components of the x, y, and z, and the Lyapunov exponential curve with parameters ξ, respectively. (b) The clustering heat-map of components in the correlation strength matrix $|R^{\mathrm{f}}|$. The components from x,y, and z are numbered in order from 1 to 201. (c) The scatter plot of entropy and participation ratio for each component.

Table 4. Percentage of components and aggregation degree in each sub-cluster for Rossler system.

(a) Frequency components						
Sub	Components from x	G_x^{sub}	Components from y	G_y^{sub}	Components from z	G_z^{sub}
s_1	17/56	1.0676	3/56	0.8799	36/56	1.0893
s_2	6/34	1.1834	3/34	1.1497	25/34	1.0180
s_3	2/36	0.4648	8/36	0.9885	26/36	0.9484
s_4	6/75	0.9887	13/75	1.0119	56/75	0.9667
(b) Scaling components						
Sub	Components from x	G_x^{sub}	Components from y	G_y^{sub}	Components from z	G_z^{sub}
s_1	12/38	0.3933	10/38	0.3330	16/38	0.5149
s_2	7/24	0.2406	11/24	0.3641	6/24	0.2103
s_3	13/34	0.4278	11/34	0.3648	10/34	0.3324

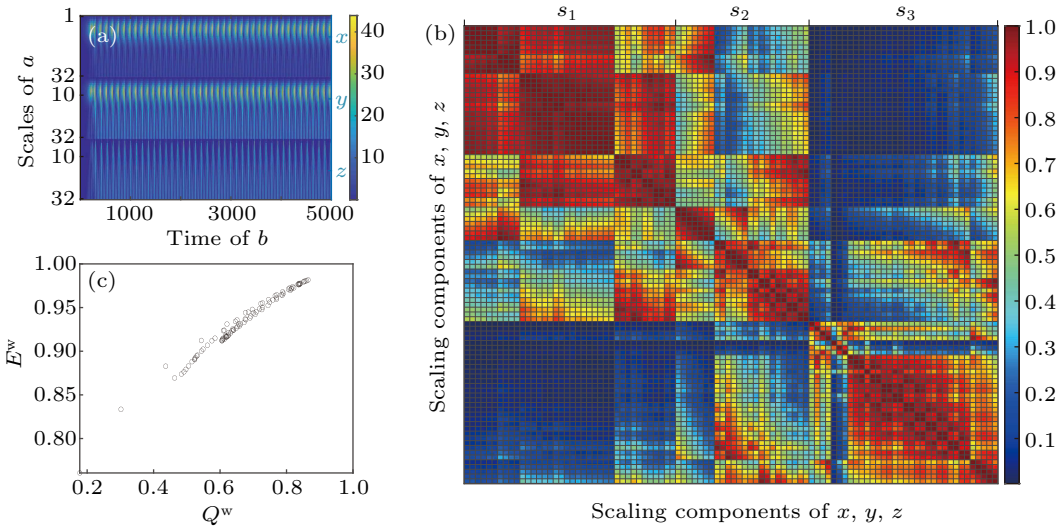


Fig. 8. Correlation between scaling components of the Rossler system. (a) The absolute values of the wavelet coefficients for x, y, and z on 32 scales, respectively. (b) The clustering heat-map of components in the correlation strength matrix $|R^{\mathrm{w}}|$. The components from x, y, and z are numbered in order from 1 to 96. (c) The scatter plot of entropy and participation ratio for each component.

For the chaotic trajectory generated with $(\mu, \nu, \xi) = (0.2, 0.2, 6.8)$, the absolute values of the wavelet coefficients for the scaling components in x (upper part), y (middle part), and z (lower part) are presented in Fig. 8(a), respectively. From Fig. 8(b), one can find that all the scaling components from x, y, and z cluster into 3 sub-clusters, named s_1, s_2, and s_3. The components in sub-cluster s_1, which has strong connections with sub-cluster s_2, is almost completely independent from s_3. From Table 4(b), one can find that the components with successive scales group tightly together in each sub-cluster. As shown in panel (c), there exists a limited number of components with low participation and entropy values. The maximum values for Q^{w} and E^{w} are 0.8650, 0.9817, whose corresponding components are the one numbered 76 from z. The scaling component numbered 76 takes as the hub of the network.

3.5. Real-wold data: Physiological signals

As a typical example, we consider the multi-channel respiratory (Resp) and ECG signal recordings from the MIMIC II matched waveform database.[49,50] The selected signal duration is 1-minute, in which a total of 7500 data points are sampled , i.e., the sampling rate is 125 Hz (see Fig. 9(a)).

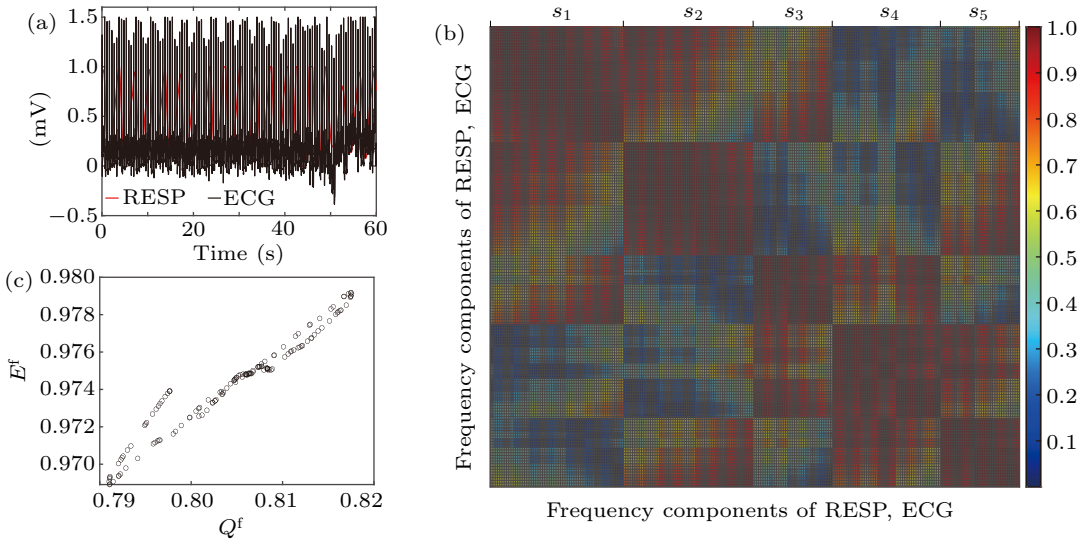


Fig. 9. Correlation between frequency components of the RESP and EEG signals. (a) The red and black curves represent the raw respiratory and ECG signals at a sampling frequency of 125 Hz for 60 seconds, respectively. (b) The clustering heat-map of components in the correlation strength matrix $|R^{\mathrm{f}}|$. The components from RESP and ECG are numbered in order from 1 to 294. (c) The scatter plot of entropy and participation ratio for each component.

The total of 294 retained frequency components, where 7 components are from Resp and 287 components are from ECG, cluster into 5 sub-clusters denoted with s_1, s_2, s_3, s_4, and s_5, respectively (see the heat-map in Fig. 9(b)). The components in sub-cluster s_1 are strongly connected to both sub-clusters s_2 and s_3, which act as centres to create links for s_2 and s_3 where limited linkages exists. At the same time, s_2 also serves as the centre for s_1 and s_5, which have limited link-

ages. Table 5(a) gives the numbers of retained frequency components and their aggregation behaviors in the (sub-)clusters each. Interestingly, three components with close frequencies numbered 1, 2, 4 from RESP take part in the formation of the sub-cluster s_1 (whose size is 74). Two components with close frequencies numbered 3, 5 from RESP appear in the sub-cluster s_2 composing of a total of 72 components. In the sub-clusters s_3 and s_5 each there appear single components from RESP numbered 6 and 7, respectively. And all the components in s_4 are from ECG. Figure 10 illustrates the network structure between the 7 frequency components of the RESP signal and the components of the ECG signal (only the 7 ECG components with strong correlation are shown) at different thresholds. One can find that as t increases, the network gradually decomposes from a highly connected state into multiple sub-clusters. When $t = 0.99$, the network exhibits the same pattern as the clustering heat-map, i.e., the components from RESP in the pink, green, orange, blue communities are attributed to sub-clusters s_1, s_2, s_3, s_5, respectively. Hence, the cross-correlation between the two signals are realized by the total 7 components from RESP, by their taking part in the four sub-clusters. Figure 9(c) gives the entropy and participation ratio for each component. The maximum values of Q^{f} and E^{f} are 0.8351, 0.9797, whose corresponding components are the ones numbered 238, 281 from EEG signals, respectively. The frequency components numbered 238, 281 take as the hubs of the network.

The absolute values of the wavelet coefficients for the scaling components in RESP (upper part) and ECG (lower part) are presented in Fig. 11(a), respectively. The scaling components group into four sub-clusters marked with s_1, s_2, s_3, and s_4 (see the heat-map in Fig. 11(b)). The sub-cluster s_4 is almost isolated with s_1, s_2, and s_3. Similarly, the sub-cluster s_3 is almost independent of sub-cluster s_1, with only limited connections to sub-cluster s_2. Table 5(b) gives also the numbers of scaling components and their aggregation behaviors in the (sub-)clusters each. In the sub-clusters s_1, s_2, and s_3 only the scaling components with successive scales from RESP signals interact with each other. While in sub-cluster s_4, there are only components from ECG signals with successive scales. Hence, the wavelet decomposition can not find the structure of cross-correlation between the two signals. As shown in panel (c), most of the points for $(Q^{\mathrm{w}}, E^{\mathrm{w}})$ cluster around the up-right corner, i.e., their values are large. The maximum values of Q^{w} and E^{w} are 0.7736, 0.9622, whose corresponding components are the ones numbered 63, 52 from ECG signals, respectively. The scaling components numbered 63, 52 take as the hubs of the network.

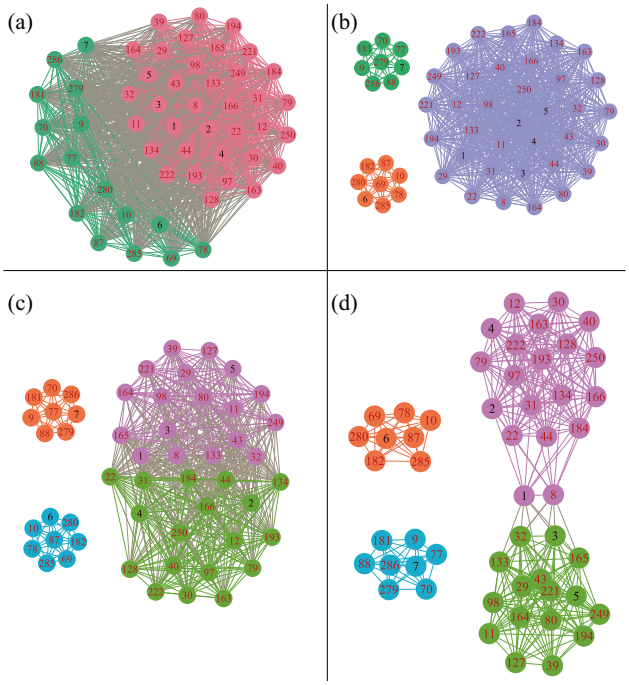


Fig. 10. Network structure between RESP signals and ECG signals. Panels (a)–(d) show strong coupling structure between the components from the RESP signal and the components from ECG signal at thresholds $t = 0$, 0.9, 0.95, 0.99, respectively. Different colours on the nodes indicate different communities. Black number: components from RESP. Red number: components from ECG.

Table 5. Percentage of components and aggregation degree in each sub-cluster for RESP and ECG.

(a) Frequency components

Sub	Components from RESP	$G^{\mathrm{sub}}_{\mathrm{RESP}}$	Components from ECG	$G^{\mathrm{sub}}_{\mathrm{ECG}}$
s_1	3/74	0.7362	71/74	0.9771
s_2	2/72	0.7471	70/72	0.9634
s_3	1/44	1	43/44	1.0362
s_4	0	0	60/60	1.0685
s_5	1/44	1	43/44	1.0125

(b) Scaling components

Sub	Components from RESP	$G^{\mathrm{sub}}_{\mathrm{RESP}}$	Components from ECG	$G^{\mathrm{sub}}_{\mathrm{ECG}}$
s_1	20/20	0.6362	0	0
s_2	6/6	0.2144	0	0
s_3	6/6	0.2096	0	0
s_4	0	0	32/32	1

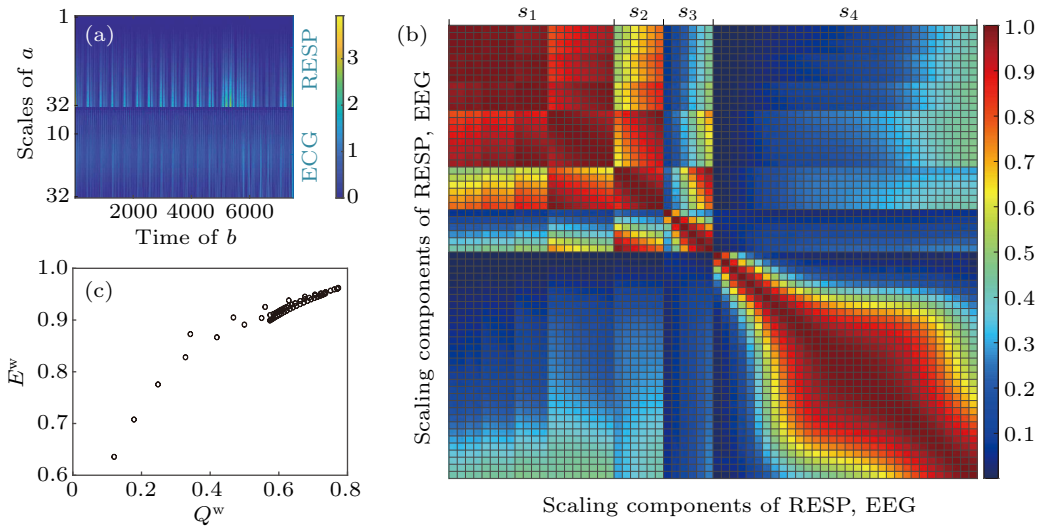


Fig. 11. Correlation between scaling components of the RESP and EEG signals. (a) The absolute values of the wavelet coefficients of RESP and EEG signals on 32 scales, respectively. (b) The clustering heat-map of components in the correlation strength matrix $|R^{\mathrm{w}}|$. The components from RESP and ECG are numbered in order from 1 to 64. (c) The scatter plot of entropy and participation ratio for each component.

4. Conclusions

In this paper, we present a theoretical framework to display the structure of (cross-)correlation between components in signals. As an illustration, the fast Fourier transform and continuous wavelet transform are adopted to decompose signals into components with different frequencies and scales, respectively. The cross-correlations between the frequency (or scaling) components form a weighted complex network.[51,52] The clustering behaviors of the network and the aggregation degrees of the components in the sub-clusters each are then used to describe the structural characteristics of the network.

Trajectories for several chaotic dynamical systems are investigated. It is found that the number of retained frequency components increases rapidly as the trajectory shifts from a non-chaotic to a chaotic state, and they group into different clusters, showing the non-trivial patterns for the cross-correlations between signals. The correlation between scaling components decays significantly along with the difference between their scales. And scaling components can only capture the patterns for intra-signal relationships.

As a typical application, we consider the coupling between the ECG and RESP signals. The cross-correlation between the two signals turn out to be realized by coupling between seven components from RESP and four sub-clusters from ECG respectively.

We hope our method are used in future to discover how the couplings between signals in reality are realized, i.e., the structure of their cross-correlation.

Acknowledgements

Project supported by the National Natural Science Foundation of China (Grant Nos. 11875042 and 11505114) and the Shanghai Project for Construction of Top Disciplines (Grant No. USST-SYS-01).

References

[1] Gao Z K, Small M and Kurths J 2017 *Europhys. Lett.* **116** 50001
[2] Hutchison R M, Womelsdorf T, Allen E A, Bandettini P A, Calhoun V D, Corbetta M, Della Penna S, Duyn J H, Glover G H, Gonzalez-Castillo J and Handwerker D A 2013 *Neuroimage.* **80** 360
[3] Scheffer M, Bascompte J, Brock W A, Brovkin V, Carpenter S R, Dakos V and Sugihara G 2009 *Nature* **461** 53
[4] Tirabassi G and Masoller C 2022 *Chaos, Solitions and Fractals* **155** 111720
[5] Patro D K, Qi M and Sun X 2013 *J. Fin. Stab.* **9** 105
[6] Dakos V, van Nes E and Scheffer M 2009 *Nat. Preced.* 1–1
[7] Ouyang F Y, Zheng B and Jiang X F 2019 *Physica A* **517** 515
[8] Moon Y I, Rajagopalan B and Lall U 1995 *Phys. Rev. E* **52** 2318
[9] Donges J F, Zou Y, Marwan N and Kurths J 2009 *Eur. Phys. J. Spec. Top.* **174** 157
[10] Wu T, Gao X, An F and Kurths J 2023 *Chaos, Solitions and Fractals* **167** 113052
[11] Lanford III O E and Ruelle D 1969 *Commun. Math. Phys.* **13** 194
[12] Rangarajan G and Ding M 2000 *Phys. Rev. E* **61** 4991
[13] Zhang M and Wang Y M 2020 *Chin. Phys. B* **29** 048901
[14] Beenakker C W 1997 *Rev. Mod. Phys.* **69** 731
[15] Edelman A and Rao N R 2005 *Acta Numer.* **14** 233
[16] Tan L, Chen J J, Zheng B and Ouyang F Y 2016 *PloS One* **11** e0149648
[17] Ouyang F Y, Zheng B and Jiang X F 2014 *Physica A* **402** 236
[18] Chen J J, Tan L and Zheng B 2015 *Sci. Rep.* **5** 8399
[19] Zhou L, Qiu L, Gu C G and Yang H J 2018 *Europhys. Lett.* **121** 48002
[20] Yan S, L S, Wang H Y, Gu C G and Yang H J 2022 *Europhys. Lett.* **138** 61001
[21] Zou Y, Donner R V, Marvan N, Donges J F and Kurths J 2019 *Phys. Rep.* **787** 1
[22] Zanin M, Papo D, Sousa P A, Menasalvas E, Nicchi A, Kubik E and Boccaletti S 2016 *Phys. Rep.* **635** 1
[23] Park H J and Friston K 2013 *Science* **342** 1238411
[24] Squartini T, Caldarelli G, Cimini G, Gabrielli A and Garlaschelli D 2018 *Phys. Rep.* **757** 1
[25] Zhang J and Small M 2006 *Phys. Rev. Lett.* **96** 238701
[26] Yang Y and Yang H J 2008 *Physica A* **387** 1381
[27] Donner RV, Zou Y, Donges JF, Marwan N and Kurths J 2010 *New J. Phys.* **12** 033025
[28] Lacasa L, Luque B, Ballesteros F, Luque J and Nuno J C 2008 *Proc. Natl. Acad. Sci. USA* **105** 4972

[29] Luque B, Lacasa L, Ballesteros F and Luque J 2009 *Phys. Rev. E* **80** 046103
[30] Ni X H, Jiang Z Q, Zhou W X 2009 *Phys. Lett. A* **373** 3822
[31] Scarsoglio S, Laio F and Ridolfi L 2013 *PloS One* **8** e71129
[32] Donges JF, Zou Y, Marwan N and Kurths J 2009 *Europhys. Lett.* **87** 48007
[33] Boers N, Goswami B, Rheinwalt A, Bookhagen B, Hoskins B and Kurths J 2019 *Nature* **566** 373
[34] Friston K J 2011 *Brain Connect.* **1** 13
[35] Bashan A, Bartsch R P, Kantelhardt J W, Havlin S and Ivanov P C 2012 *Nat. Commun.* **3** 702
[36] Bartsch R P, Liu K K, Bashan A and Ivanov P C 2015 *PloS One* **10** e0142143
[37] Ma L, Chen M, He A, Cheng D and Yang X 2023 *Chin. Phys. B* **32** 100501
[38] Buckner R L and DiNicola L M 2019 *Nat. Rev. Neurosci.* **20** 593
[39] Liu K L, Bartsch R P, Ma Q D and Ivanov P C 2015 *J. Phys. Conf. Ser.* **640** 012013
[40] Haluszczynski A, Laut I, Modest H and Rath C 2017 *Phys. Rev. E* **96** 062315
[41] Tipton C 2022 *Johnson Matthey Technol. Rev.* **66** 169
[42] Cooley J W and Tukey J W 1965 *Math. Comput.* **19** 297
[43] Torrence C and Compo G P 1998 *Bull. Am. Meteorol. Soc.* **79** 61
[44] Suarez D A and Salazar A 2009 *Opt. Commun.* **282** 4203
[45] Xu X, Zhang J and Small M 2008 *Proc. Natl. Acad. Sci. USA* **105** 19601
[46] Tumminello M, Aste T, Di Matteo T and Mantegna R N 2005 *Proc. Natl. Acad. Sci. USA* **102** 10421
[47] Zhang J, Luo X, Nakamura T, Sun J and Small M 2007 *Phys. Rev. E* **75** 016218
[48] Donner R V, Small M, Donges J F, Marwan N, Zou Y, Xiang R X and Kurths J 2011 *Int. J. Bifurcat. Chaos* **21** 1019
[49] Pimentel M A, Johnson A E, Charlton P H, Birrenkott D, Watkinson P J, Tarassenko L and Clifton D A 2016 *IEEE T. Bio-Med. Eng.* **64** 1914
[50] Goldberger A L, Amaral L A, Glass L, Hausdorff J M, Ivanov P C, Mark R G and Stanley H E 2000 *Circulation* **101** e215
[51] Gao Z K and Jin N D 2009 *Phys. Rev. E* **79** 066303
[52] McCullough M, Small M, Stemler T and Lu H H C 2015 *Chaos* **25** 053101